Tunneling anisotropic magnetoresistance in C_{60}-based organic spintronic systems

K. Wang, J. G. M. Sanderink, T. Bolhuis, W. G. van der Wiel, and M. P. de Jong*

NanoElectronics Group, MESA + Institute for Nanotechnology, University of Twente, P.O. Box 217, Enschede, 7500AE, The Netherlands

(Received 19 February 2014; published 16 May 2014)

C_{60} fullerenes are interesting molecular semiconductors for spintronics since they exhibit weak spin-orbit and hyperfine interactions, which is a prerequisite for long spin lifetimes. We report spin-polarized transport in spin-valve-like structures containing ultrathin (<10 nm) C_{60} layers, ferromagnetic (FM) epitaxial face-centered-cubic (fcc) Co (111) contacts, AlO_x tunnel barriers, and nonmagnetic Al counter electrodes. Even though genuine spin-valve behavior cannot occur for only one FM contact, we find significant tunneling anisotropic magnetoresistance (TAMR) upon rotating the in-plane magnetization, originating from spin-orbit interaction (SOI) induced anisotropy of the fcc (111) Co bands. The uniaxial magnetocrystalline anisotropy of the Co electrodes results in a predominantly twofold symmetric in-plane TAMR effect. We investigated the TAMR effect in the direct tunneling regime (2 nm C_{60}), at the transition point to two-step tunneling (4 nm C_{60}), and in the multistep regime (8 nm C_{60}). A sizable TAMR of 4.5% is found at 5 K under application of a 500-mT in-plane magnetic field for C_{60} layers of 2 nm, which is strongly suppressed at 8 nm thickness, indicating that TAMR may strongly contribute to the "spin-valve" signal for direct tunneling, but not for multistep tunneling. The TAMR effect is proposed to be due to a combination of SOI induced modulation of the tunneling DOS upon rotating the in-plane magnetization of the fcc epitaxial Co thin film, resonant tunneling processes involving interfacial states, and different Bychkov-Rashba SOI at the different interfaces.

DOI: 10.1103/PhysRevB.89.174419 PACS number(s): 85.75.−d, 75.76.+j, 81.05.Fb, 85.30.Mn

I. INTRODUCTION

The field of semiconductor spintronics aims at information processing using the spin polarization of charge carriers in semiconductors. The main advantage of using carbon-based, organic semiconductors (OSCs) for spintronics lies in their light chemical constituents (i.e., C and H) which have been expected to yield weak spin-orbit interaction (SOI), such that the spin orientation of electrons and holes may be retained for a long time [1,2]. Combined with their chemical tunability, mechanical flexibility, light weight, and low cost processing, which drive the fast developing field of organic electronics, a bright future may lie ahead for OSCs in spintronic applications. An important milestone in the field was the demonstration of giant magnetoresistance at low temperature in organic spin-valve structures [3,4].

The magnetoresistance (MR) devices usually consist of two ferromagnetic (FM) leads separated by an organic semiconductor acting as tunnel barrier or charge and spin transport spacer. A considerable MR can be obtained, by switching the magnetization vectors of the FM electrodes, and therefore their spin quantization axes, from parallel to antiparallel. In spite of this success, the operation principle of organic spin valves is not well understood. A frequently overlooked, but highly relevant tunneling phenomenon, in which the tunneling transmission depends on the magnetization direction with respect to the crystallographic axes of the ferromagnet(s), is known as tunneling anisotropic magnetoresistance (TAMR). Recently, the TAMR effect has been reported in an organic-based system, i.e., $La_{0.7}Sr_{0.3}MnO_3$(LSMO)/PTCDI-C4F7/Ti/Au [5]. A detailed analysis of the spin-valve-like signal showed a correlation with the biaxial anisotropy of the LSMO bottom electrode. This study illustrates the importance of TAMR with respect to MR effects in (organic) spin valves, especially when crystalline FMs are involved, and shows the need to distinguish TAMR effects from genuine spin-valve effects arising from spin-dependent transmission through two FM interfaces.

One remarkable feature of TAMR is that only one FM contact is needed [6,7]. This offers the possibility to investigate to what extent TAMR, originating from a single FM interface, contributes to "spin-valve" behavior. Here, we address this question for C_{60}-based spin valves with face-centered-cubic (fcc) Co (111) electrodes, by studying devices that contain a single FM electrode (Co), and a nonmagnetic counter electrode (Al). Our recent experiments on fcc-Co(111)/AlO_x/Al tunnel junctions showed sizable TAMR ratios, of approximately 7.5% and 11% at 5 K, for the in- and out-of-plane configurations, respectively [8]. Here, we investigate how the TAMR evolves with the insertion of 2–8-nm C_{60} layers in the junctions. Our previous work on vertical C_{60}-based spin valves (containing two FM contacts) has shown that the electronic transport and MR can be described by a multistep tunneling model for such ultrathin C_{60} layers [9]. At a C_{60} thickness of about 3–4 nm, a transition occurs from direct tunneling to two-step (or multistep) tunneling via C_{60}-derived states. In this work, we report TAMR effects in the direct tunneling regime (2 nm C_{60}), at the transition point to two-step tunneling (4 nm C_{60}), and in the multistep regime (8 nm C_{60}).

The first observation of TAMR in spintronic devices [GaAs/(Ga,Mn)As/AlO_x/Ti/Au junctions] has demonstrated clear spin-valve-like signals, and an in-plane TAMR ratio of approximately 2.7% at 4.2 K was found [7]. The key concept revealed by this work is that the orientation of the magnetization affects the (interfacial) spin-dependent density of states (DOS) via the anisotropic SOI in the ferromagnetic lattice. Following this approach, other systems, which often utilized semiconductors with zinc blende structure, such as GaAs and ZnSe, as a tunneling barrier or spacer in conjugation with ferromagnetic (Ga, Mn)As, have shown in-plane TAMR

*Corresponding author: m.p.dejong@utwente.nl

effects at low temperatures [10–12]. In such structures, the noncentrosymmetric zinc blende structure (of, e.g., GaAs) and asymmetry in the device configuration (producing potential steps at the interfaces) lead to an interplay between Dresselhaus SOI and Bychkov-Rashba SOI that determines the resulting TAMR [13,14]. A clear twofold symmetric TAMR is obtained for the in-plane geometry, which originates from the in-plane anisotropic characteristics of the SOI field. Another class of devices in which TAMR has been studied in some detail is magnetic tunnel junctions (MTJs) with bcc FM electrodes (e.g., Fe, CoFe). For example, TAMR in CoFe-based MTJs, containing both MgO and Al_2O_3 barriers, have shown twofold and fourfold symmetric signals, depending on the bias voltage, when the magnetization rotates from in plane to out of plane [15]. In such structures, the effect of the Bychkov-Rashba SOI on resonant tunneling through surface states mostly probably produces the effects. TAMR has also been observed down to the atomic scale, e.g., for single Co atoms adsorbed on magnetic domains and domain walls of a Fe/W multilayer thin film [16]. By scanning tunneling spectroscopy (STM), the TAMR was found to be as large as 12%, while the effect repeatedly changed sign as a function of bias voltage. Other investigations also involve break junctions [17,18], nanoconstrictions [19,20], and nanocontacts [21].

The overall content of this work is organized as follows. Section II provides the experimental details. Section III contains the results and discussion of magnetotransport studies of the TAMR effect in sapphire(substrate)/Co/AlO_x/C_{60}/Al systems.

II. EXPERIMENTAL DETAILS

All spintronic devices were fabricated *in situ* in an ultrahigh vacuum (UHV, base pressure 10^{-10} mbar) electron beam (*e*-beam) evaporation system with an integrated load-lock chamber. The C_{60} layer was grown using a temperature-controlled Knudsen cell. One-side-polished monocrystalline sapphire wafers (0001), diced into 11 × 11 mm^2 pieces, were used as substrates. Prior to the device fabrication, the substrate was cleaned in ultrasonic baths of acetone and isopropanol at 45 °C. Epitaxial Co layers, with a thickness of 8 nm, were deposited through a shadow mask (to form 2 × 5 mm^2 strips) onto the sapphire substrates at room temperature. The in-plane epitaxial relation between the 8 nm Co film and the substrate is shown in Fig. 1(a). Growth at room temperature produces

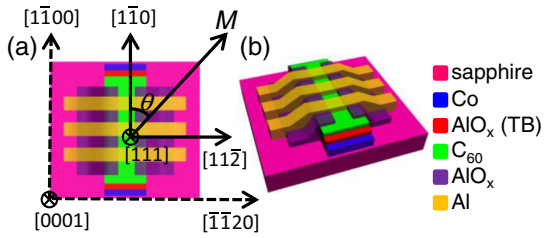

FIG. 1. (Color online) Schematic diagrams of (a) top view of the spintronic device with structure Co(8 nm)/AlO_x(3.3 nm)/C60/Al (35 nm), with crystallographic directions shown of the single crystalline sapphire substrate and the epitaxial 8-nm Co thin film; (b) three-dimensional view of the device structure.

a purely fcc crystalline structure of the Co layer. More details about the growth mode of Co on sapphire can be found in Refs. [22,23]. Subsequently, a 2.5-nm thin Al layer was evaporated on top of the Co thin film, with a deposition rate of approximately 1 Å/s. In order to produce an amorphous AlO_x tunneling barrier, the sample was transferred into the load-lock chamber, and exposed to 30 min plasma oxidation, under an oxygen pressure of 100 mTorr at room temperature. This oxidation process results in 3.3 nm AlO_x. Afterwards, C_{60} layers were thermally evaporated from a Knudsen cell at 400 °C, with an evaporation rate of 2 nm/min. AlO_x layers of 30 nm thickness were deposited through a shadow mask to define a narrow (250 μm) strip on the Co/AlO_x/C_{60} stack, by *e*-beam evaporation from Al_2O_3 source material. Finally, the junctions were defined by depositing 35-nm-thick Al strips through a shadow mask, to form cross-bar structures with 250 × 300 μm^2 junction areas. A schematic drawing of the device structure is depicted in Fig. 1(b).

Magnetotransport measurements were performed with a liquid helium flow cryostat equipped with a 1-T electromagnet. A four-wire measuring method was adopted to minimize the contributions from lead or contact resistances. The spintronic devices were mounted onto a sample holder that enables 360° in-plane rotation. The spin-valve-like TAMR signals were measured by sweeping the magnetic field within ±150 mT, while injecting a constant dc current through the devices. The angle-dependent TAMR measurements were carried out by keeping the magnetic field strength large enough (i.e., B = 500 mT) for reaching in-plane magnetization saturation of the Co layer; meanwhile, a constant dc current was injected through the junction, and the corresponding voltage was recorded with a nanovoltmeter at 5 K.

III. RESULTS AND DISCUSSION

We start with magnetotransport measurements on a junction containing a 2-nm C_{60} layer, for which electronic transport can be described by direct tunneling between the metal electrodes [as opposed to two-step (or multistep) tunneling via C_{60}-derived states]. In Ref. [8], we have reported large TAMR in Co/AlO_x/Al junctions, fabricated in the same way as the devices described in this work, but without the additional layer of C_{60} molecules [8]. Since the electrons (mostly) tunnel in a single step through the composite barrier consisting of the AlO_x film plus the 2-nm C_{60} layer, the effects of adding the C_{60} molecules between the AlO_x barrier and the Al electrode of a Co/AlO_x/Al junction can be ascribed to the modification of the electronic structure at the C_{60}/Al interface, and a change in the barrier height and width.

Figure 2 shows the I-V characteristics of an organic spintronic device with structure sapphire/Co(8 nm)/AlO_x(3.3 nm)/C_{60}(2 nm)/Al(35 nm), measured at temperatures ranging from 300 to 5 K under a bias of ±200 mV. All measurements show nonlinear and quasisymmetric behavior with respect to zero bias. The junction resistance is weakly influenced by the temperature, consistent with the notion that the transport takes place via (direct) tunneling. The near-parabolic differential conductance curve, measured at 5 K (top inset), further confirms this. The normalized zero bias resistance (ZBR, i.e., dI/dV at V = 0 V) was measured to be

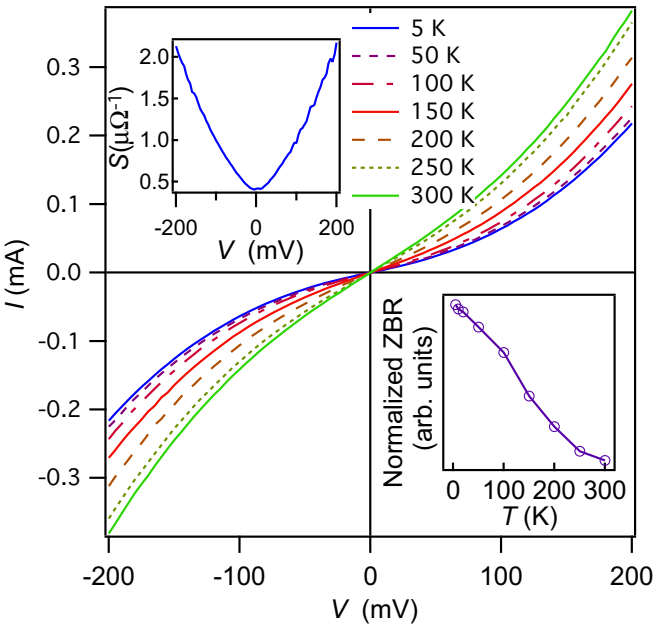

FIG. 2. (Color online) Temperature dependence of I-V measurements for sapphire/Co(8 nm)/AlO_x(3.3 nm)/C_{60}(2 nm)/Al(35 nm) junctions; left inset: the conductance versus bias voltage measured at 5 K; right inset: temperature-dependent normalized zero bias resistance (NZBR).

approximately 920 Ω at 5 K. The temperature dependence of the normalized ZBR, displayed in the bottom inset of Fig. 1, shows weak insulatorlike behavior, which indicates tunneling through a pinhole and defect free barrier.

Figures 3(a)–3(e) display the MR measurements across the junctions for the in-plane configuration at five different temperatures, 200, 100, 50, 10, and 5 K, respectively. Even though the device contains only a single ferromagnetic electrode, spin-valve-like features with distinct switching events for magnetic field sweeps in opposite directions can be observed at temperatures below 100 K. At higher temperatures (i.e., above 100 K), such signals cannot be observed. The magnitude of the switching field is about 3.8 mT at 5 K, which is slightly larger than the coercivity of the 8-nm fcc Co thin film (i.e., 2.7 mT) grown on the sapphire substrate (0001) at room temperature [8].

The spin-valve-like signals originate from TAMR, as we show by in-plane TAMR measurements, carried out by measuring the resistance while the magnetization is oriented along different in-plane crystallographic axes or k vectors of the epitaxial Co thin film. The corresponding schematic illustration is shown in Fig. 1(a). In this case, the direction of current flow across the junction is always perpendicular to the magnetization. The [$1\bar{1}0$] crystallographic direction (i.e., the magnetic easy axis) of the epitaxial Co thin film was chosen as the reference axis. The corresponding TAMR ratio can then be calculated as [24]

$$\mathrm{TAMR}(\theta) = \frac{R_{[ijk]}(\theta) - R_{[1\bar{1}0]}(0)}{R_{[1\bar{1}0]}(0)}, \qquad (1)$$

where θ is the angle between the magnetization vector and the [$1\bar{1}0$] axis. The thus obtained TAMR measurements of the

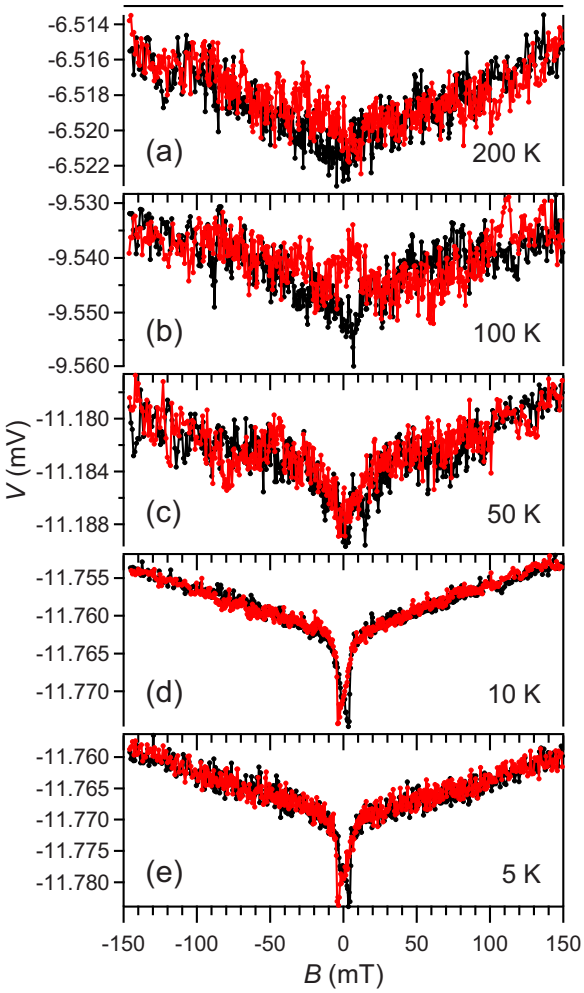

FIG. 3. (Color online) Temperature dependence of in-plane hysteresis magnetoresistance curves measured at (a) 200 K, (b) 100 K, (c) 50 K, (d) 10 K, and (e) 5K for sapphire/Co(8 nm)/AlO_x(3.3 nm)/C_{60}(2 nm)/Al(35 nm) junctions, respectively.

sapphire/Co(8 nm)/AlO_x(3.3 nm)/C_{60}(2 nm)/Al(35 nm) layer stack are presented in Fig. 4. Figure 4(a) shows a contour plot for the in-plane TAMR ratios as a function of both in-plane angle (θ) and bias current (I) at 5 K, under application of a 500-mT in-plane magnetic field. Two pairs of dark and bright regions, which represent relatively large TAMR ratios of opposite sign, can be seen within the full 360° range of in-plane magnetization rotations. Both of these features are strongest close to the zero bias current, and show a clear twofold symmetry centered at about 180°.

The largest in-plane TAMR ratio that we observed in this system is approximately equal to 4.5%. This is smaller than the 7.5% TAMR effect for similar junctions without C_{60} layers, but still considerable. Some selected plots showing the bias and angle dependence of the TAMR ratios are given in Figs. 4(b)–4(e). From Figs. 4(b) and 4(c), it is clear that the TAMR ratio decreases strongly and monotonically with the increasing bias current. The trends are generally similar to those observed for Co/AlO_x/Al junctions. Another similarity for junctions with and without the 2-nm C_{60} interlayer is the predominantly twofold symmetric TAMR at low bias (see Figs. 4(d), 4(e),

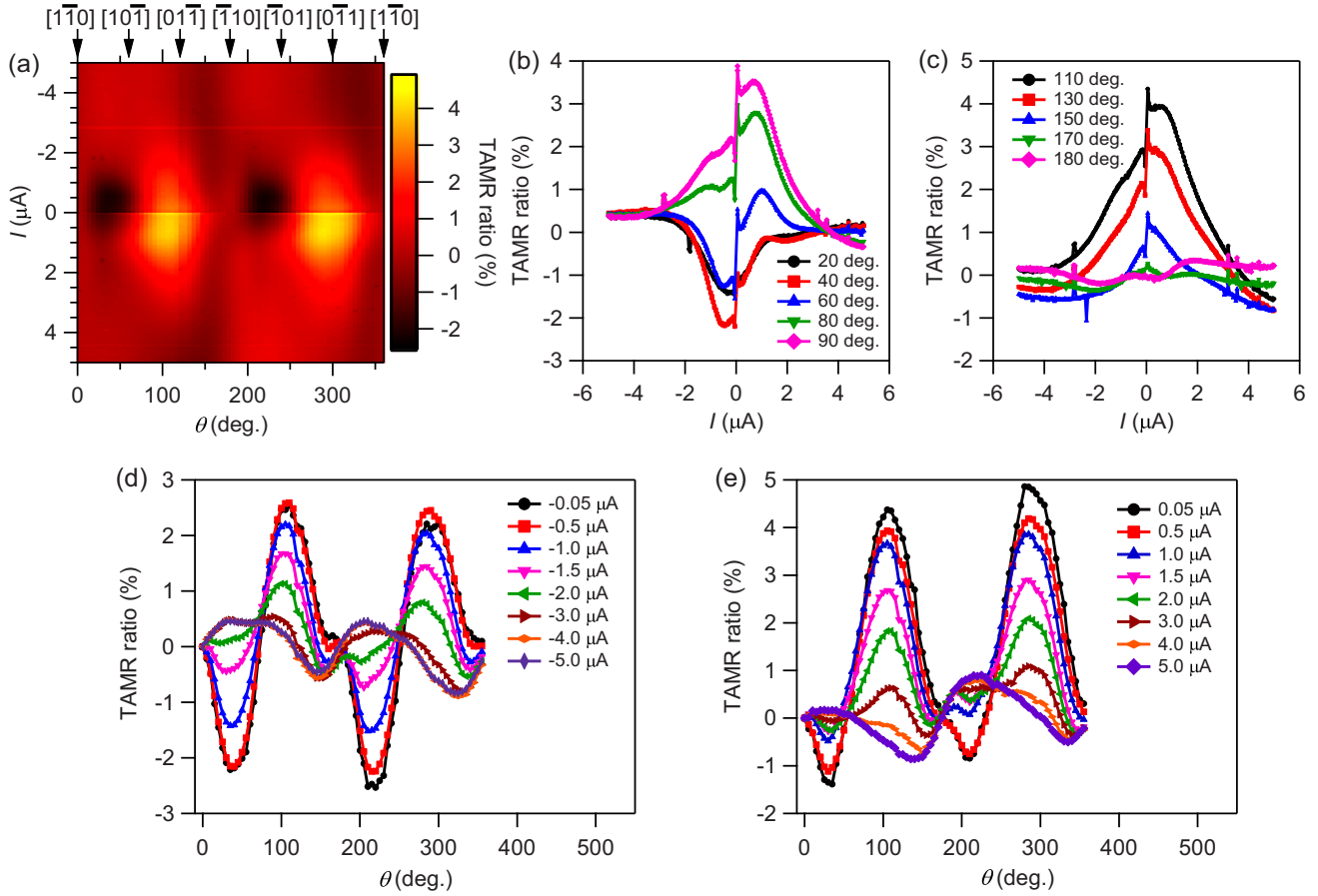

FIG. 4. (Color online) An organic spintronic device with structure, sapphire/Co(8 nm)/AlO_x(3.3 nm)/C_{60}(2 nm)/Al(35 nm). (a) Contour plot of the TAMR ratio as a function of both applied bias current and in-plane magnetization angle, measured at 5 K under application of a constant magnetic field of 500 mT. The color in the contour plot represents the magnitude of the TAMR ratio in percent (see color bar). (b) and (c) show TAMR versus bias current for several different angles from 0 to 180°. (d) and (e) are angle dependence of TAMR for negative and positive bias current, respectively.

6(c), and 6(d) of Ref. [8]) [7,8], including the shoulders at approximately 180° and 360°. Besides these similarities, there are also some marked differences. At low bias (i.e., $-2\ \mu\text{A} \leqslant I \leqslant 2\ \mu\text{A}$), corresponding to $-7\ \text{mV} \leqslant V \leqslant 7\ \text{mV}$, the in-plane magnetization angle for which the tunneling resistance is lowest has shifted by about 30°. For Co/AlO_x/Al junctions, the minimum junction resistance was found when the magnetization was oriented along the [**1$\bar{1}$0**] direction ($\theta = 0$); this is no longer the case for the Co/AlO_x/C_{60}(2 nm)/Al junctions [8]. Instead, in Figs. 4(d) and 4(e), one can observe that the TAMR varies from negative to positive, with the largest negative values occurring for negative bias current. This implies that the resistance of the junction firstly decreases, and then starts to increase when the magnetization rotates away from the easy axis (i.e., the [**1$\bar{1}$0**] crystallographic direction) of the Co thin film.

Another difference compared to the Co/AlO_x/Al junctions is the strong bias dependence at different in-plane angles. As shown in Figs. 4(d) and 4(e), when the bias current level exceeds ±2.0 μA (i.e., ±7 mV), the TAMR-θ curves change considerably and different features start to emerge. Consequently, at high bias, the maxima and minima in the TAMR appear at different angles than at low bias. Such effects were not observed in Co/AlO_x/Al junctions, where the main effect of increasing the bias was only a continued suppression of the TAMR. The different behavior of the two sets of devices can be attributed to the different electronic structure of the C_{60}/Al interface as compared to the AlO_x/Al interface. Although the TAMR originates from the anisotropic SOI at the Co/AlO_x interface, the tunneling rates depend on the electronic structure on both sides of the barrier.

Another effect that must be considered is that the addition of the C_{60} layer impacts the Bychkov-Rashba SOI at the interface with the Al electrode. The AlO_x and C_{60} layers form two different interfaces on either side of the junction, corresponding to effective Bychkov-Rashba SOI changes. This, as a consequence, affects the TAMR. The tunneling current I that flows across the junction under an externally applied bias V can then be written as [24,25]

$$I = \frac{e}{(2\pi)^3\hbar}\sum_{\sigma=\uparrow\downarrow}\int T_\sigma(E-eV,k_{||})\{f_l(E-eV) - [1-f_r(E)]\}dEd^2k_{||}, \quad (2)$$

where e is the electron charge, $\hbar$ is Plank's constant divided by 2π, σ denotes the spin up ($\sigma = \uparrow$) and down ($\sigma = \downarrow$)

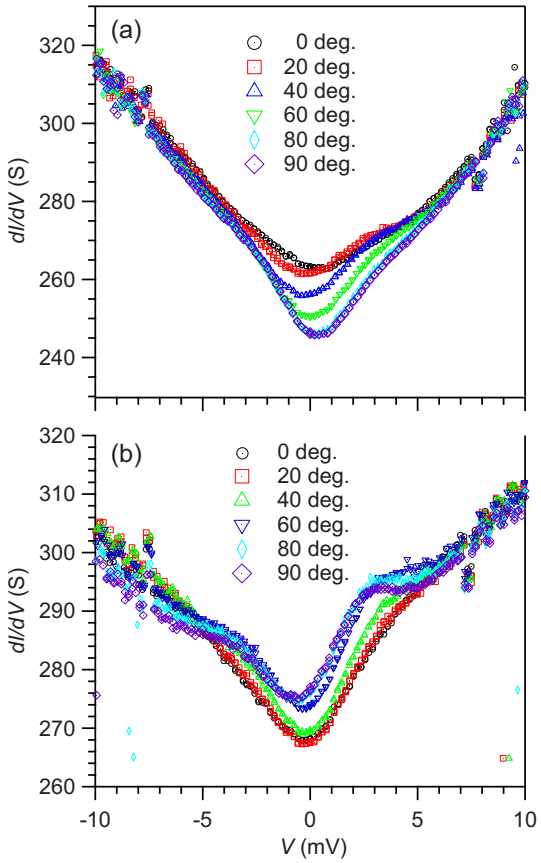

FIG. 5. (Color online) Differential conductance measured at 5 K under application of a constant magnetic field of 500 mT for (a) the reference device sapphire/Co(8 nm)/AlO_x(3.3 nm)/Al(35 nm) and (b) sapphire/Co(8 nm)/AlO_x(3.3 nm)/C_{60}(2 nm)/Al(35 nm).

states, and $f_l(E)$ and $f_r(E)$ correspond to the Fermi-Dirac distributions in the left and right metallic (or ferromagnetic) electrodes, respectively. $k_\parallel$ denotes the wave vectors (k_x, k_y) in the plane of the layers. $T_\sigma(E, k_\parallel)$ represents the transmissivity which depends on the Rashba parameters, V, and spin orientation [24,25]. Meanwhile, the bias can alter the Bychkov-Rashba parameter $\tilde{\alpha}$ across the potential barrier, because this parameter strongly depends on the strength of the electrical field along the growth direction. The TAMR vanishes when the Bychkov-Rashba parameter $\tilde{\alpha} = 0$ [24,25]. Previous studies using ferromagnets Co_2MnSi and $Co_{50}Fe_{50}$ show remarkably different TAMR features when different interfacial structures were considered [26]. In addition, Gao *et al*. demonstrated that the same magnetic tunnel junctions with different tunneling barriers, Al_2O_3, and MgO yielded a completely different bias and angle dependence of the TAMR effect [15].

Further effects of the interfacial electronic structure modification due to the presence of the C_{60} molecules in the junction can be observed in differential conductance (dI/dV) measurements which were performed at 5 K in a 500-mT magnetic field applied at different in-plane angles. Figures 5(a) and 5(b) show the differential conductance spectra measured at some selected angles, for devices without (i.e., Co/AlO_x/Al) and with 2-nm C_{60} thin molecular films in the junctions, respectively. Both plots show asymmetric conductance spectra for all the selected angles, due to the asymmetry of the (occupied and unoccupied) DOS of the electrodes and their interfaces. In addition, the unequal magnitudes of the Co and Al work functions affect the potential barrier profile, which introduces additional asymmetry. The variation of the conductance with θ for small bias (i.e., $-7\ \text{mV} < V < +7\ \text{mV}$, or $-2\ \mu\text{A} < I < +2\ \mu\text{A}$, under application of a constant magnetic field strength) reveals the anisotropic tunneling behavior. For a bias larger than ± 7 mV, the conductance shows a linearly increasing trend. Within the bias current range from $+7$ mV to -7 mV, where the largest TAMR occurs, one narrow dip around zero bias and two shoulders at approximately ± 3 mV are observed.

The differences between the conductance spectra of Figs. 5(a) and 5(b) can again be attributed to the different interfaces in the device; upon including C_{60} molecules in the junctions hybridized electronic states at the Al/C_{60} interface are expected. Indeed, many studies of C_{60}/Al interfaces reveal strong chemical interactions and (partial) charge transfer [27]. The direct evaporation of Al onto C_{60} leads to chemical reactions, accompanied by electron donation from Al to C_{60} molecules. Previously reported photoelectron spectroscopy (PES) measurements have shown the formation of π^*-derived interfacial states close to E_F, due to partial occupancy of the lowest unoccupied molecular orbital (LUMO) of C_{60}. These interfacial states strongly affect the tunneling characteristics, as is clearly revealed from a comparison between Figs. 5(a) and 5(b).

We now briefly address the two magnetic field-dependent shoulders in the conductance spectra of Figs. 5(a) and 5(b). Since the Al electrode is nonmagnetic, the electronic structure (i.e., DOS) of the fcc Co electrode should be responsible. In Fig. 5(a), a negative bias corresponds to electrons injected from Co to Al, which involves occupied states in the Co electrode. The states that are increasingly localized start to contribute as the bias increases, which results in the shoulder [28]. Such a phenomenon becomes more remarkable in even thinner fcc Co layers, and it seems to be a signature of fcc Co [29,30]. Similar effects can be seen for positive bias voltages, when electrons tunnel into the Co unoccupied states above the Fermi energy. The difference in the conductance spectra in Figs. 5(a) and 5(b) can be attributed to the contribution of (resonant) states at the C_{60}/Al interface in (b), while the evolution of the features with magnetic field angle mainly reflects the uniaxial magnetocrystalline anisotropy of the epitaxial fcc Co.

Figure 6 displays the TAMR measurements for a device with structure sapphire/Co(8 nm)/AlO_x(3.3 nm)/C_{60}(4 nm)/Al(35 nm). For a 4-nm C_{60} layer, two-step tunneling processes, via intermediate states in the C_{60} layer, start to play a significant role in addition to direct tunneling [9]. This turns out to have a strong effect on the TAMR of the junctions. The contour plot of Fig. 6(a) depicts the TAMR as a function of bias and in-plane magnetization angle. The main features still show a twofold symmetry within the 360° in-plane rotation of the magnetization, originating from the anisotropic SOI of the Co/AlO_x interface, but are otherwise quite different from those observed for devices with 2 nm C_{60} (or Co/AlO_x/Al reference devices). The shoulders on the main features can no longer be observed, and, notably, the TAMR ratios are predominantly

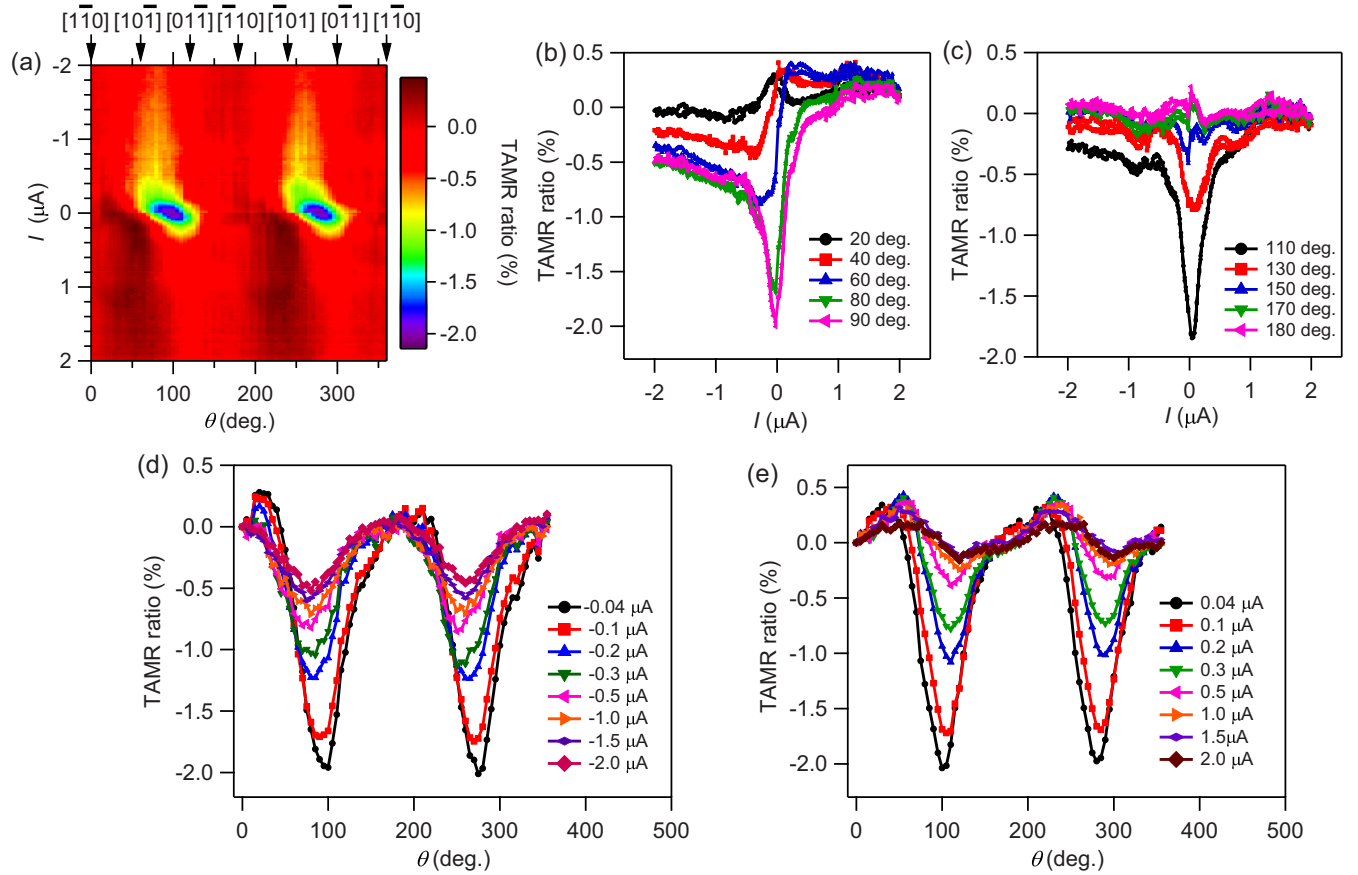

FIG. 6. (Color online) An organic spintronic device with structure, sapphire/Co(8 nm)/AlO_x(3.3 nm)/C_{60}(4 nm)/Al(35 nm). (a) Contour plot of the TAMR ratio as a function of both applied bias current and in-plane magnetization angle, measured at 5 K under application of a constant magnetic field of 500 mT. The color in the contour plot represents the magnitude of the TAMR ratio in percent (see color scale). (b) and (c) show TAMR versus bias current for several different angles from 0 to 180°. (d) and (e) are angle dependence of TAMR for negative and positive bias current, respectively.

negative, meaning that the tunneling resistance is largest when the magnetization is oriented along the magnetic easy axis [$1\bar{1}0$]. The maximum TAMR ratio is approximately equal to −2%, which is almost two times smaller than that of the device with a 2-nm C_{60} layer. Figures 6(b) and 6(c) show the TAMR ratios as a function of the bias current. In comparison with Figs. 4(b) and 4(c), the bias dependence of the TAMR of the device with a 4-nm C_{60} layer is exceptionally strong, and significant (>0.5%) signals occur only within a narrow bias current window of $\pm 1\mu$A (i.e., ±3.4 mV).

Further increase of the C_{60} layer thickness up to 8 nm leads to a continued strong suppression of the TAMR effect, as is shown in Fig. 7(a). For such "thick" C_{60} layers, direct tunneling from Co to Al (or vice versa) no longer contributes significantly to the current; instead charge transport takes place via one or several intermediate states in the C_{60} layer. The resulting TAMR signals are very small (on the order of 0.1%), except for a sharp peak of about 1.5%, within a very narrow bias current window of ±0.4 μA. In Figs. 7(b) and 7(c), no significant differences can be found in the bias dependence of the TAMR for different magnetization angles. The results in Figs. 7(a), 7(d), and 7(e) reveal, at negative bias currents of −0.2 μA or larger, a TAMR effect that is qualitatively similar to that observed for the device with 4 nm C_{60} (two dips at about 90° and 270°), while no clear TAMR effect can be discerned for positive bias. This is consistent with the observation that the TAMR effect for the device with 4 nm C_{60} falls off much more rapidly for positive bias than for negative bias.

IV. CONCLUSION

We have investigated the in-plane TAMR effect in junctions consisting of sapphire/Co(8 nm)/AlO_x(3.3 nm)/C_{60}/Al(35 nm). The effects are proposed to be due to a combination of SOI induced modulation of the tunneling DOS upon rotating the in-plane magnetization of the fcc epitaxial Co thin film, resonant tunneling processes at the interfaces (e.g., C_{60}/Al), and different Bychkov-Rashba SOI at the different interfaces. The TAMR, which was measured at 5 K under application of a 500-mT magnetic field, decreased from 4.5% to 1.5% as the thickness of C_{60} was changed from 2 to 8 nm, coinciding with a transition from direct to multistep tunneling through the C_{60} layer. The in-plane angle dependence of the TAMR measurements reveals a clear twofold symmetry. We have addressed the crucial role played by the various interfaces in the junctions, underlining that the (spin-dependent) interfacial DOS has a distinct influence on the TAMR effects.

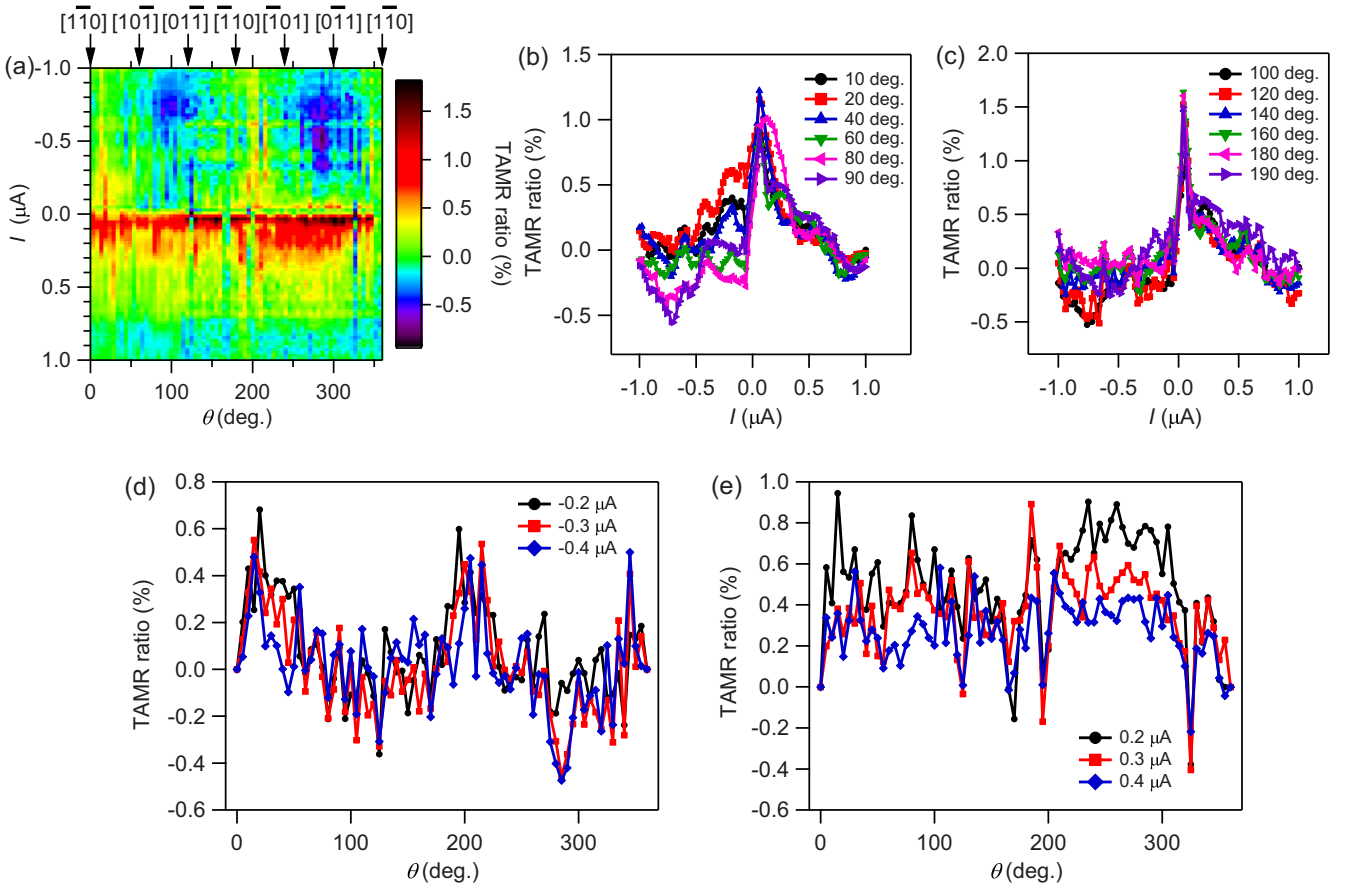

FIG. 7. (Color online) An organic spintronic device with structure, sapphire/Co(8 nm)/AlO_x(3.3 nm)/C_{60}(8 nm)/Al(35 nm). (a) Contour plot of the TAMR ratio as a function of both applied bias current and in-plane magnetization angle, measured at 5 K under application of a constant magnetic field of 500 mT. The color in the contour plot represents the magnitude of the TAMR ratio in percent (see color scale). (b) and (c) show TAMR versus bias current for several different angles from 0 to 180°. (d) and (e) are the TAMR angle dependence for negative and positive bias current, respectively.

ACKNOWLEDGMENTS

We acknowledge financial support from the European Research Council (ERC Starting Grant No. 280020), and the research program of the Foundation for Fundamental Research on Matter (FOM, Grant No. 10PR2808), which is part of the Netherlands Organization for Scientific Research (NWO).

[1] V. A. Dediu, L. E. Hueso, I. Bergenti, and C. Taliani, Nat. Mater. **8**, 707 (2009).
[2] V. Vardeny, Nat. Mater. **8**, 91 (2009).
[3] D. Sun, L. Yin, C. Sun, H. Guo, Z. Gai, X. G. Zhang, T. Z. Ward, Z. Cheng, and J. Shen, Phys. Rev. Lett. **104**, 236602 (2010).
[4] Z. H. Xiong, D. Wu, Z. Valy Vardeny, and J. Shi, Nature **427**, 821 (2004).
[5] M. Grünewald, M. Wahler, F. Schumann, M. Michelfeit, C. Gould, R. Schmidt, F. Würthner, G. Schmidt, and L. W. Molenkamp, Phys. Rev. B **84**, 125208 (2011).
[6] C. Rüster, C. Gould, T. Jungwirth, E. Girgis, G. M. Schott, R. Giraud, K. Brunner, G. Schmidt, and L. W. Molenkamp, J. Appl. Phys. **97**, 10C506 (2005).
[7] C. Gould, C. Rüster, T. Jungwirth, E. Girgis, G. M. Schott, R. Giraud, K. Brunner, G. Schmidt, and L. W. Molenkamp, Phys. Rev. Lett. **93**, 117203 (2004).
[8] K. Wang, T. L. A. Tran, P. Brinks, J. G. M. Sanderink, T. Bolhuis, W. G. van der Wiel, and M. P. de Jong, Phys. Rev. B **88**, 054407 (2013).
[9] T. L. A. Tran, T. Q. Le, J. G. M. Sanderink, W. G. van der Wiel, and M. P. de Jong, Adv. Funct. Mater. **22**, 1180 (2012).
[10] J. Moser, A. Matos-Abiague, D. Schuh, W. Wegscheider, J. Fabian, and D. Weiss, Phys. Rev. Lett. **99**, 056601 (2007).
[11] C. Rüster, C. Gould, T. Jungwirth, J. Sinova, G. M. Schott, R. Giraud, K. Brunner, G. Schmidt, and L. W. Molenkamp, Phys. Rev. Lett. **94**, 027203 (2005).
[12] H. Saito, S. Yuasa, and K. Ando, Phys. Rev. Lett. **95**, 086604 (2005).
[13] G. Dresselhaus, Phys. Rev. **100**, 580 (1955).
[14] Y. A. Bychkov and E. I. Rashba, J. Phys. C **17**, 6039 (1984).
[15] L. Gao, X. Jiang, S.-H. Yang, J. D. Burton, E. Y. Tsymbal, and S. S. P. Parkin, Phys. Rev. Lett. **99**, 226602 (2007).

[16] N. Néel, S. Schröder, N. Ruppelt, P. Ferriani, J. Kröger, R. Berndt, and S. Heinze, Phys. Rev. Lett. **110**, 037202 (2013).
[17] K. I. Bolotin, F. Kuemmeth, and D. C. Ralph, Phys. Rev. Lett. **97**, 127202 (2006).
[18] J. D. Burton, R. F. Sabirianov, J. P. Velev, O. N. Mryasov, and E. Y. Tsymbal, Phys. Rev. B **76**, 144430 (2007).
[19] A. D. Giddings, M. N. Khalid, T. Jungwirth, J. Wunderlich, S. Yasin, R. P. Campion, K. W. Edmonds, J. Sinova, K. Ito, K. Y. Wang, D. Williams, B. L. Gallagher, and C. T. Foxon, Phys. Rev. Lett. **94**, 127202 (2005).
[20] M. Ciorga, M. Schlapps, A. Einwanger, S. Geissler, J. Sadowski, W. Wegscheider, and D. Weiss, New J. Phys. **9**, 351 (2007).
[21] D. Jacob, J. Fernández-Rossier, and J. J. Palacios, Phys. Rev. B **77**, 165412 (2008).
[22] O. Yabuhara, M. Ohtake, Y. Nukaga, and M. Futamoto, in *2nd International Symposium on Advanced Magnetic Materials and Applications*, edited by M. Takahashi, H. Saito, S. Yoshimura, K. Takanashi, M. Sahashi, and M. Tsunoda, Vol. 266 (IOP Publishing Ltd, Bristol, 2011), p. 012049.
[23] M. Ohtake, O. Yabuhara, Y. Nukaga, and M. Futamoto, in *Joint European Magnetic Symposia*, edited by J. Spalek, Vol. 303 (IOP Publishing Ltd, Bristol, 2011), p. 012016.
[24] A. Matos-Abiague and J. Fabian, Phys. Rev. B **79**, 155303 (2009).
[25] A. Matos-Abiague, M. Gmitra, and J. Fabian, Phys. Rev. B **80**, 045312 (2009).
[26] T. Uemura, M. Harada, K.-i. Matsuda, and M. Yamamoto, Appl. Phys. Lett. **96**, 252106 (2010).
[27] D. W. Owens, C. M. Aldao, D. M. Poirier, and J. H. Weaver, Phys. Rev. B **51**, 17068 (1995).
[28] P. LeClair, J. T. Kohlhepp, C. H. van de Vin, H. Wieldraaijer, H. J. M. Swagten, W. J. M. de Jonge, A. H. Davis, J. M. MacLaren, J. S. Moodera, and R. Jansen, Phys. Rev. Lett. **88**, 107201 (2002).
[29] P. LeClair, H. J. M. Swagten, J. T. Kohlhepp, and W. J. M. de Jonge, Appl. Phys. Lett. **76**, 3783 (2000).
[30] P. LeClair, H. J. M. Swagten, J. T. Kohlhepp, R. J. M. van de Veerdonk, and W. J. M. de Jonge, Phys. Rev. Lett. **84**, 2933 (2000).